The Cryosphere, 4, 583–592, 2010
www.the-cryosphere.net/4/583/2010/
doi:10.5194/tc-4-583-2010


The Cryosphere

# A sea-ice thickness retrieval model for 1.4 GHz radiometry and application to airborne measurements over low salinity sea-ice

**L. Kaleschke**[1], **N. Maaß**[1], **C. Haas**[2], **S. Hendricks**[3], **G. Heygster**[4], **and R. T. Tonboe**[5]

[1]Institute of Oceanography, University of Hamburg, Bundesstraße 53, 20146 Hamburg, Germany
[2]Department of Earth & Atmospheric Sciences, University of Alberta Edmonton, Alberta T6G 2E3, Canada
[3]Alfred Wegener Institute for Polar and Marine Research, Bussestr. 24, 27570 Bremerhaven, Germany
[4]Institute of Environmental Physics, University of Bremen, P.O. Box 330440, Germany
[5]Center for Ocean & Ice, Danish Meteorological Institute, Lyngbyvej 100, 2100 Copenhagen, Denmark

Received: 19 October 2009 – Published in The Cryosphere Discuss.: 18 November 2009
Revised: 7 June 2010 – Accepted: 24 November 2010 – Published: 13 December 2010

**Abstract.** In preparation for the European Space Agency's (ESA) Soil Moisture and Ocean Salinity (SMOS) mission, we investigated the potential of L-band (1.4 GHz) radiometry to measure sea-ice thickness.

Sea-ice brightness temperature was measured at 1.4 GHz and ice thickness was measured along nearly coincident flight tracks during the SMOS Sea-Ice campaign in the Bay of Bothnia in March 2007. A research aircraft was equipped with the L-band Radiometer EMIRAD and coordinated with helicopter based electromagnetic induction (EM) ice thickness measurements.

We developed a three layer (ocean-ice-atmosphere) dielectric slab model for the calculation of ice thickness from brightness temperature. The dielectric properties depend on the relative brine volume which is a function of the bulk ice salinity and temperature.

The model calculations suggest a thickness sensitivity of up to 1.5 m for low-salinity (multi-year or brackish) sea-ice. For Arctic first year ice the modelled thickness sensitivity is less than half a meter. It reduces to a few centimeters for temperatures approaching the melting point.

The campaign was conducted under unfavorable melting conditions and the spatial overlap between the L-band and EM-measurements was relatively small. Despite these disadvantageous conditions we demonstrate the possibility to measure the sea-ice thickness with the certain limitation up to 1.5 m.

The ice thickness derived from SMOS measurements would be complementary to ESA's CryoSat-2 mission in terms of the error characteristics and the spatiotemporal coverage. The relative error for the SMOS ice thickness retrieval is expected to be not less than about 20%.

*Correspondence to:* L. Kaleschke
(lars.kaleschke@zmaw.de)

## 1 Introduction

Soil Moisture and Ocean Salinity (SMOS) is an earth observation mission developed by the European Space Agency (ESA) launched on 2 November 2009. NASA's Aquarius mission is planned to follow in 2011. Their main objectives are to provide global measurements of soil moisture over land and sea surface salinity over ocean from L-band (frequency $f$=1.4 GHz; wavelength $\lambda$=21 cm) radiometric observations.

An exciting spin-off is the retrieval of sea-ice thickness which was expected to be possible due to the large penetration depth at L-band (Mätzler, 2001). These new L-band radiometers could provide sea-ice thickness information complementary to that from altimeters because of the expected sensitivity to thin ice thickness variations. Moreover, they would provide near real-time data with an almost global coverage every second day which is important for operational applications such as weather prediction and ship routing. Thin ice up to 0.4 m dominates the ocean-atmosphere heat exchange in the Arctic during the cold months (Maykut, 1978) and is important for the large-scale sea-ice rheology (Feltham, 2008).

Published by Copernicus Publications on behalf of the European Geosciences Union.

Menashi et al. (1993) have demonstrated the possibility of ice thickness retrieval for radiometric measurements at 0.6 GHz. In this article, we describe the adaption of their model for the conditions encountered in the Baltic Sea. The model will be used for the analysis of L-band radiometric and EM ice thickness measurements which were obtained in the Bothnian Bay in March 2007 as part of the first SMOS sea-ice campaign.

The Microwave Imaging Radiometer using Aperture Synthesis (MIRAS), the SMOS payload, is based on a novel technique for passive microwave aperture synthesis inspired from radio astronomy (Corbella et al., 2004). MIRAS does not measure the brightness temperature of the scene, but its Fourier spectrum by the correlation of 69 individual antennas. The inversion of the spectrum leads to a field of view with hexagon-like shape and a nadir resolution of about 35 km. The complex imaging geometry is different from previous satellite radiometers. The MIRAS priniciple allows multi-angle observations within an alias-free field-of-view (FOV), analogue to the swath width, of at the most 1000 km. The resolution decrease to about 80 km in the far range (Kerr et al., 2001).

The specific aim of this study is the investigation of the thermal microwave radiation emitted by a homogeneous closed ice cover at 1.4 GHz. We try to answer the following questions: how can we measure ice thickness from the observed brightness temperature, in which thickness range and with what accuracy? How are the results influenced by the ice temperature and salinity? Will there be an advantage of SMOS compared to CryoSat-2 for sea-ice thickness measurement?

To answer these questions only very limited data are available. The SMOS Sea-Ice field campaign in the Baltic Sea during the mild March 2007, so far provided the only measurements of 1.4 GHz brightness temperature together with the ice thickness. Therefore, we restrict the discussion to low salinity ice at high temperatures which was observed during this particular field campaign. However, the model presented in the following could be applied for the Arctic and Antarctic as well. As the model is designed for retrieval, we have to make a number of simplifications to reduce the number of free parameters. A comparison with models of higher complexity has been conducted in the framework of the ESA SMOS-Ice project and is covered in the final report (Heygster et al., 2009).

In Sect. 2 of this paper, a model for the partly sea-ice covered ocean emissivity is introduced. A simplified retrieval version is presented in Sect. 3. In Sect. 4 the data from the SMOS Sea-Ice field campaign are described. In Sect. 5 the results from sensitivity studies and from the validation are shown. The retrieval uncertainties are discussed and generalized for SMOS and CryoSat-2 in Sect. 6. Finally, Sect. 7 concludes this paper.

## 2 Emissivity model for 1.4 GHz

In our model, we assume only two surface types, open water and ice with the fractional area coverage (total ice concentration) $1-C$ and $C$, respectively. The observed brightness temperature at the surface depends on the temperatures of water $T_{\mathrm{water}}$ and ice $T_{\mathrm{ice}}$ and their emissivities $e_{\mathrm{water}}$ and $e_{\mathrm{ice}}$. Furthermore, $T_{\mathrm{obs}}$ is a function of the incidence angles and the polarisation. Without loss of generality, we will restrict our discussion to the nadir case

$$T_{\mathrm{obs}} = (1-C)e_{\mathrm{water}}T_{\mathrm{water}} + Ce_{\mathrm{ice}}T_{\mathrm{ice}}. \quad (1)$$

Here, we neglect the atmospheric contribution, ionospheric effects, cosmic and solar radiation (Reul et al., 2008; Tenerelli et al., 2008). The latter terms are important for sea surface salinity retrieval with demanding requirements on the radiometer's accuracy. However, all terms are relatively small compared to the large brightness contrast between water and thick ice which cover a 150 K range from 90 K to 240 K. For sea surface salinity retrieval, one has to utilize a much narrower range covering only a few K or even tenths of a K.

For a specular reflecting surface the horizontal and vertical nadir components are equal. It is not possible to derive two parameters, thickness and concentration, from only one nadir measurement of the brightness temperature. Thus, it is necessary to prescribe the ice concentration. In the following, we limit the discussion to a closed ice cover with $C \approx 1$.

### 2.1 Open water

The emissivity of the water surface $e_{\mathrm{water}}$ is calculated from the Fresnel equations (Swift, 1980). We apply the model of Klein and Swift (1976) for the permittivity of sea water. The nadir brightness temperature of the ocean surface close to the freezing point is $92 \pm 1$ K for salinities between 33 and 35, e.g., in the Arctic marginal ice zone, and $96 \pm 1$ K in the northern Baltic Sea where surface salinities range between 2 and 7 (Leppäranta and Myrberg, 2009). Following the recommendations of UNESCO (1985), the salinity is referenced with no units.

At L-band the sensitivity of wind-induced surface roughness is as small as 0.2 K per 1 m/s (Dinnat and Boutin, 2003). Thus, the wind influence can certainly be neglected for the aim of sea-ice thickness retrieval.

### 2.2 Sea-ice emissivity

Brine pockets and air bubbles are much smaller than the L-band wavelength of 21 cm. Therefore, the sea-ice can be considered as a homogeneous medium which greatly simplifies the set-up of an emissivity model at 1.4 GHz. The emissivity of ice $e_{\mathrm{ice}}$ follows from considering reflection at a dielectric slab of ice over water. The reflection coefficient of an ice slab over an infinite half plane can be expressed as a function of

the reflection coefficients $R_1$ and $R_2$, describing reflection at the upper and lower boundary of the slab (Ulaby et al., 1981):

$$R = \frac{R_1 + R_2 e^{-2ik_{i,z}d}}{1 + R_1 R_2 e^{-2ik_{i,z}d}}, \quad (2)$$

where $d$ is ice thickness and $k_{i,z}$ is the z-component of the propagation vector in ice $\boldsymbol{k_i}$, with the z-axis perpendicular to the slab. The expression for $k_{i,z}$ can be separated into its real part $\beta$, which is called the phase constant, and its imaginary part $\alpha$, which is referred to as the attenuation coefficient: $k_{i,z} = \beta - i\alpha$. The expressions for $\alpha$ and $\beta$ are

$$\alpha = \frac{\omega}{c_0} \cos\theta_i \, |Im\sqrt{\epsilon_i}| \quad (3)$$

$$\beta = \frac{\omega}{c_0} \cos\theta_i \, Re\sqrt{\epsilon_i}, \quad (4)$$

with the angle of refraction $\theta_i$ in the ice, the relative permittivity of ice $\epsilon_i$, the angular frequency $\omega = 2\pi f$ and the speed of light $c_0$ in vacuum. The ice emissivity is calculated from $e_{\mathrm{ice}} = 1 - r = 1 - R\overline{R}$, where $r$ is reflectivity and $\overline{R}$ is the conjugate-complex of the reflection coefficient $R$. Assuming real power reflection coefficients the following expression for ice emissivity was derived (Menashi et al., 1993):

$$e_{\mathrm{ice}} = \frac{(1-r_i)(1-Ar_w)}{1 + Ar_i r_w + 2\sqrt{Ar_i r_w}\cos(2\beta d)}, \quad (5)$$

where $A = \mathrm{e}^{-4\alpha \mathrm{d}}$. The reflectivity of air to ice $r_i$ and the reflectivity of ice to water $r_w$ are calculated from the Fresnel equations with the permittivity of ice provided in the next section.

The above equation is a coherent solution describing ice emissivity as a periodic function of ice thickness. If the rms thickness variation of the ice slab is sufficiently large, i.e., more than a quarter of the used electromagnetic wavelength over the illumination footprint, the periodicity averages out and an incoherent solution can be introduced instead. The emissivity of ice averaged over a variety of ice thicknesses was derived by Menashi et al. (1993) and can be expressed as follows:

$$e_{\mathrm{ice}} = \frac{(1-r_i)(1-Ar_w)}{1 - Ar_i r_w} \left[ \frac{1 - \sqrt{Ar_i r_w}\mathrm{e}^{-\beta\sigma_\mathrm{d}}}{1 + \sqrt{Ar_i r_w}\mathrm{e}^{-\beta\sigma_\mathrm{d}}} \right], \quad (6)$$

where $\sigma_d$ is rms thickness variation (roughness). The equations presented in Menashi et al. (1993) contain the optical pathlength $l$ and its variation $\sigma_l$ instead of ice thickness $d$ and thickness variation $\sigma_d$ in Eq. (6). This is a small mistake of Menashi et al. (1993) and contradictory to Ulaby et al. (1981). The expressions for the attenuation coefficient $\alpha$ and the phase coefficient $\beta$ used by Menashi et al. (1993) do not take into account the cosine term, which originates from considering the z-component of the propagation vector only (Eqs. 3, 4). However, this mistake has only a minor effect and the scientific results obtained by Menashi et al. (1993) remain unquestioned.

The transition of open water to a very thin ice cover falls outside the assumptions for the incoherent solution. However, we assume that a smooth connection of the open water emissivity and the valid part of the model is reasonable.

**Table 1.** Coefficients for the calculation of the sea-ice dielectric constant (Hallikainen and Winebrenner, 1992). The 1.4 GHz coefficients are linearly interpolated.

| Frequency [GHz] | $a_1$ | $a_2$ | $a_3$ | $a_4$ |
|---|---|---|---|---|
| First year ice | | | | |
| 1.0 | 3.12 | 0.0090 | 0.039 | 0.00504 |
| 1.4 | 3.10 | 0.0084 | 0.037 | 0.00445 |
| 2.0 | 3.07 | 0.0076 | 0.034 | 0.00356 |
| Multi year ice | | | | |
| 1.0 | 3.12 | 0.0090 | −0.004 | 0.00436 |
| 1.4 | 3.10 | 0.0084 | 0.003 | 0.00435 |
| 2.0 | 3.07 | 0.0076 | 0.013 | 0.00435 |

**Table 2.** Polynomial coefficients for the calculation of the brine volume (Leppäranta and Manninen, 1988).

| | $\alpha_0$ | $\alpha_1$ | $\alpha_2$ | $\alpha_3$ |
|---|---|---|---|---|
| $F_1$ | −0.041221 | −18.407 | 0.58402 | 0.21454 |
| $F_2$ | 0.090312 | −0.016111 | 0.00012291 | 0.00013603 |

### 2.2.1 Sea-ice permittivity

Vant et al. (1978) proposed an empirical relationship for the permittivity of ice depending on the relative brine volume (in ‰; valid for $V_b < 70$‰):

$$\epsilon_{\mathrm{ice}} = a_1 + a_2 V_b + i(a_3 + a_4 V_b), \quad (7)$$

A linear combination of the coefficients derived at 1 and 2 GHz (Table 1) is used as an approximate value for 1.4 GHz. Leppäranta and Manninen (1988) derived equations for determining the relative brine volume of low-salinity ice for temperatures between −2°C and 0°C

$$V_b = \frac{\rho_i S_{\mathrm{ice}}}{F_1(T) - \rho_i S_{\mathrm{ice}} F_2(T)}. \quad (8)$$

Table 2 gives the coefficients of the polynomials $F = \sum_{j=0}^{3} \alpha_j T^j$. The pure ice density $\rho_i$ is 917 kg/m$^3$. Winter bulk ice salinity averaged over samples collected at landfast sea-ice in the Gulf of Finland in 1999–2001 is $S_{\mathrm{ice}} = 0.65 \pm 0.3$ (Granskog et al., 2004). For more saline ice and lower temperatures, the equations of Cox and Weeks (1983) and Frankenstein and Garner (1967) are applied instead.

## 3 A semi-empiric retrieval model

Several relatively simple empiric or semi-empiric models have been successfully applied for the retrieval of sea-ice concentration from passive microwave sensors (Andersen et al., 2007). The inverse retrieval problem is, in general,

ill-posed. The following simplifications are a way to constrain the inverse problem with a priori knowledge, namely the assumption about sea-ice concentration, temperature and salinity. In the following, we describe a semi-empiric formulation that could later be used for the satellite retrieval.

An approximation of the emissivity model (Eqs. 1, 6) is given by the following expression

$$T_{\mathrm{obs}} = T_m - (T_m - T_0)\exp(-\gamma d), \tag{9}$$

with the brightness temperature of open water $T_0$ and an attenuation factor $\gamma$. The mixture brightness temperature $T_m$ is defined as

$$T_m = CT_1 + (1-C)T_0, \tag{10}$$

with the brightness temperature of infinitely thick ice $T_1$ and ice concentration $C$.

Equation (9) can directly be inverted for the retrieval of ice thickness

$$d = -\frac{1}{\gamma}\ln\left(\frac{T_m - T_{\mathrm{obs}}}{T_m - T_0}\right). \tag{11}$$

The most important error characteristic is defined by the condition $T_{\mathrm{obs}} + \delta > T_1$ which defines the maximum ice thickness $d_{\mathrm{max}}$ that can be retrieved for a given observational error $\delta$. Towards this limit the errors become infinitely large and asymmetric. The resulting maximum ice thickness is given in Sect. 5.1.4.

The three parameters $T_0$, $T_1$ and $\gamma$ can be obtained either from an emissivity model as described in the previous Sect. 2 or from brightness temperatures and corresponding ice thickness measurements as outlined in Sect. 6.

## 4 Measurements

Measurements of the brightness temperature at 1.4 GHz and the sea-ice thickness were conducted nearly simultaneously in the Bothnian Bay on 12 and 13 March 2007. The Helsinki University of Technology (HUT) SkyVan research aircraft was equipped with the Technical University of Denmark (DTU) National Space Institute Radiometer (EMIRAD). The non-imaging EMIRAD measurements were coordinated with helicopter EM ice thickness measurements. The air temperature measured at Hailuoto increased from an average of $-6\,^{\circ}$C on the 5 March to an average above $0\,^{\circ}$C on 12 and 13 March. Photographs taken during the flights show features that look like a very wet surface or even like ponded ice (Fig. 4).

### 4.1 L-band radiometer EMIRAD

EMIRAD measures the fully polarimetric state of the electromagnetic emission (Rotbøll et al., 2003). The radiation was measured with two antennas, one with a nadir beam and the other with an aft looking beam with an angle of incidence of $40\,^{\circ}$. The footprint of the nadir measurement at a flight level of 1000 m is about 680 m. The radiometer data were provided with a sampling rate of 125 Hz. The signal was integrated over 200 samples leading to an oversampled footprint spacing of approximately 90–100 m.

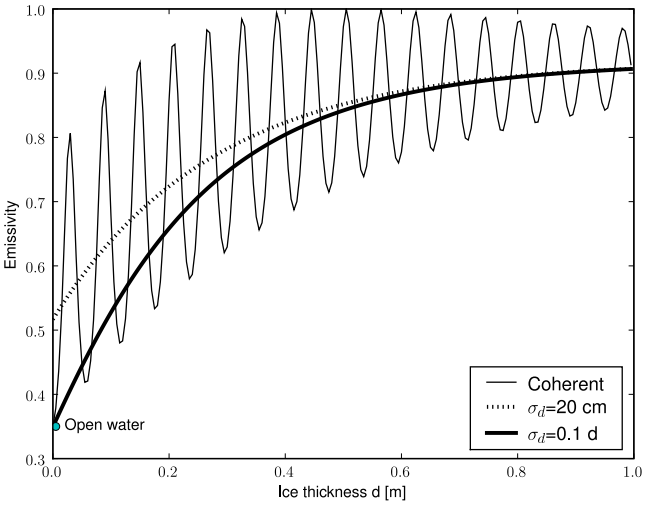


**Fig. 1.** Nadir 1.4 GHz emissivity of a slab of Baltic sea-ice ($S = 0.65$, $T = -2\,^{\circ}$C). The coherent and two incoherent solutions are shown for two different parameterizations of the thickness roughness $\sigma_d$. The open water emissivity is indicated with the filled circle.

The EMIRAD data were found to be occasionally degraded due to unstable behaviour of the power converter. This caused deviations from the nominal performance of the radiometer and introduced spikes and jumps in the data. The brightness temperature signals were carefully investigated and obviously degraded sections were removed from the analysis.

### 4.2 Electromagnetic induction system

A system of a transmitter and receiver coil operating at 3.68 kHz is towed by helicopter and is used to estimate sea-ice thickness (Haas et al., 2009). The footprint of a single measurement is about 40 m, while the recording frequency of 10 Hz results in a point spacing of 3–4 m at typical speeds of a helicopter. The general accuracy over level ice is $\pm$ 10 cm. Over ridged areas the error can increase to about 50% of ice thickness. Additional errors can arise in shallow brackish waters (Haas, 2004; Hendricks and Haas, 2009).

## 5 Results

### 5.1 Model sensitivity study

The modelled brightness temperature mainly depends on polarisation, incidence angle, ice concentration, ice thickness, ice and water salinities, ice and water temperatures and

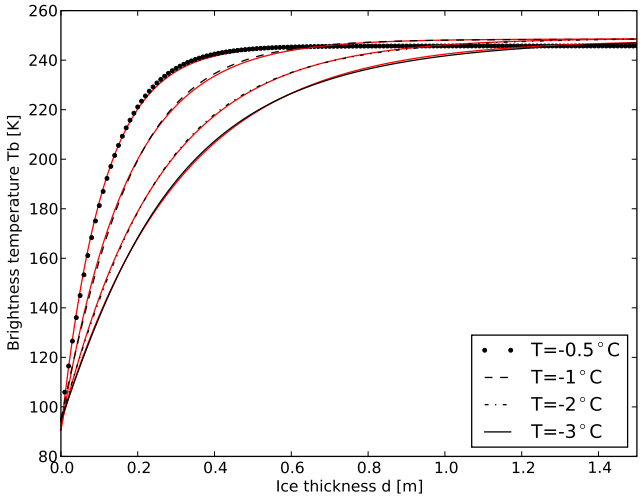


**Fig. 2.** Nadir 1.4 GHz brightness temperature of Baltic sea-ice ($S = 0.65$, roughness $\sigma_d = 0.1d$) for different ice temperatures. The results of the semi-empiric model (Eq. 9) are indicated with the red lines.

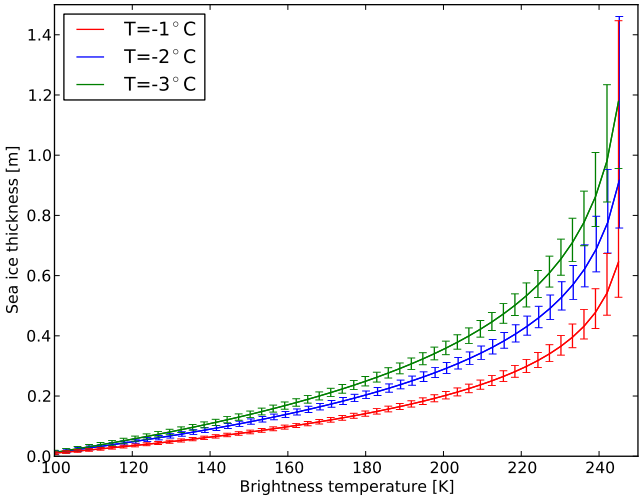


**Fig. 3.** Model inversion for the retrieval of the ice thickness from the brightness temperature. The error bars indicate ± 3.5 K variations of the brightness temperature which corresponds to a 5% error of ice concentration.

sea-ice roughness. Here, we restrict the investigation to the nadir ice thickness retrieval for ice concentration near 100%. The most important free parameters are the ice and the water salinity and temperature, as well as the ice roughness. In the following, we keep the water salinity and temperature fixed at $S_{\text{water}} = 2$ and $T_{\text{water}} = 0°\text{C}$ and vary the ice roughness, temperature and salinity.

### 5.1.1 Sea-ice roughness

The sea-ice roughness $\sigma_d$ influences the asymptotic behaviour of the emissivity model towards zero ice thickness. The resulting emissivities for two different parameterizations of $\sigma_d$ are shown together with the coherent solution (Eq. 5) in Fig. 1. The coherent solution for the emissivity of a plane-parallel ice slab over an infinite half plane reduces to the emissivity of open water for a vanishing ice thickness as expected.

The incoherent solution for a constant positive $\sigma_d$ does not converge to the emissivity of open water, which reveals this choice as not admissible. To circumvent this problem, we introduce a parameterization of $\sigma_d$ as a fixed percentage of ice thickness. This is a reasonable assumption because the thickness variability, in general, increases with the thickness. The incoherent form (Eq. 6) with this parameterization approaches the emissivity of open water. In the following, the ad hoc assumption $\sigma_d = 0.1d$ is applied with the incoherent model.

### 5.1.2 Sea-ice temperature and salinity

The resulting brightness temperatures for different sea-ice bulk temperatures and salinities are shown in Fig. 2. For Baltic sea-ice with $S = 0.65$ the brightness temperature levels out at about $d = 0.5$ m for $T_{\text{ice}} = -0.5°$ C and at $d = 1.5$ m for $T_{\text{ice}} = -2°$C. For $T_{\text{ice}} = -3°$ C the penetration depth is approximately 1.5 m for these low salinity conditions. For typical Arctic or Antarctic first year ice with $T_{\text{ice}} = -5°$ C and $S = 8$ the resulting brightness temperature (not shown) resembles that of the Baltic sea-ice at $T_{\text{ice}} = -0.5°$ C.

### 5.1.3 Retrieval model approximation

The results of the semi-empiric model are shown in Fig. 2 together with the results of the emissivity model. The parameters $T_0$, $T_1$ or $T_m$ and $\gamma$ have been obtained by least squares optimization. For example, the resulting parameters for ice concentration $C = 1$, ice temperature $T_{\text{ice}} = -2°$ C, ice salinity $S = 0.65$ and the roughness parameterization $\sigma_d = 0.1d$ are $T_0 = 92.3$ K, $T_m = T_1 = 248.9$ K and $\gamma = 4.0$. The accuracy of the retrieval model approximation is better than ± 1 K for $d > 0.1$ m and $C > 0.5$. Thus, it is a good assumption for the major part of the ice covered seas.

### 5.1.4 Maximum retrievable ice thickness

The maximum ice thickness $d_{\text{max}}$ follows from the definition in Sect. 3. For Baltic sea-ice at $T = -3°$C the maximum thickness is $d_{\text{max}} \approx 1.5$ m for an assumed measurement uncertainty $\delta = 1$ K. It reduces to 0.9 m for Baltic sea-ice at a temperature of $T = -1°$C. For more saline Arctic first year ice ($S \approx 8$) at $T = -3°$C, the maximum ice thickness is less than half a metre.

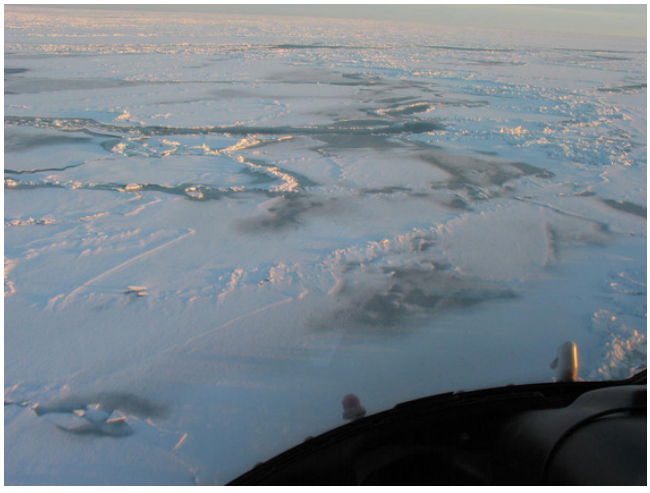

**Fig. 4.** Melted surface on the flight of 13 March 2007. Photograph courtesy of Juha Karvonen (FIMR).

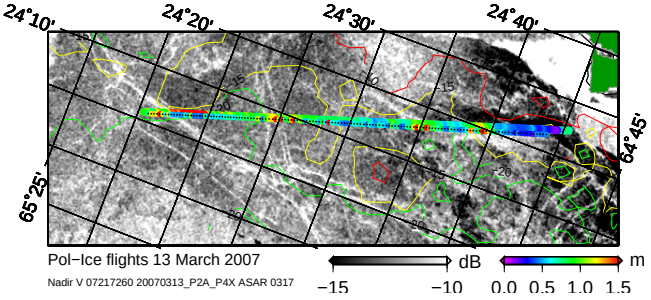


**Fig. 5.** Flight track of 13 March 2007 and the colour coded thickness overlaid on a ASAR WSM image of 17 March 2007. The smaller dots indicate the helicopter EM and the larger dots the Sky-Van EMIRAD measurements. The size of the footprints are not in scale. The bathymetry is indicated with the red (10 m), yellow (15 m), and green (20 m) isolines. The island Hailuto is in the upper right corner in green colour.

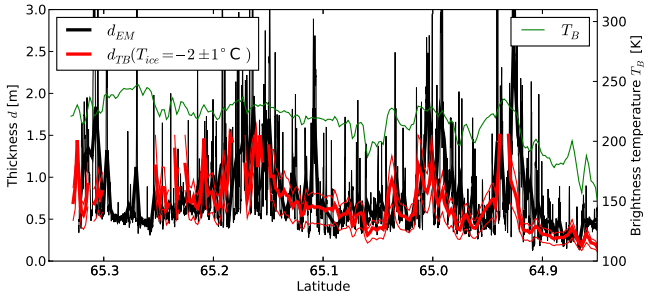


**Fig. 6.** Thickness retrievals and brightness temperature from the flight of 13 March 2007. The graph shows the EM-thickness $d_{\mathrm{EM}}$ and the thickness $d_{\mathrm{TB}}$ derived from the brightness temperature for the prescribed ice temperature $T_{\mathrm{ice}} = -2 \pm 1\,^{\circ}\mathrm{C}$. The thin black line represents the EM-thickness at 40 m resolution while the thick line is a running average over about 1200 m. The red lines indicate the L-band thickness retrieval including the sensitivity rage for a $\pm 1^{\circ}\mathrm{C}$ temperature changes. Data gaps in the red ($d_{\mathrm{TB}}$) curve indicate failures of the retrieval method.

### 5.1.5 Sensitivity of the retrieval

The sensitivity of the retrieval to variations in temperature and radiometric accuracy is shown in Fig. 3. For example, a variation in the ice temperature by $\pm 1\,^{\circ}\mathrm{C}$ around a mean temperature of $-2\,^{\circ}\mathrm{C}$ results in a deviation of $\pm 0.05$ m for $d = 0.2$ m ($T_{\mathrm{obs}} = 180$ K) and in a deviation of $\pm 0.1$ m for $d = 0.4$ m ($T_{\mathrm{obs}} = 220$ K). An uncertainty in the radiometric accuracy of $\pm 1$ K leads to a thickness uncertainty of $\pm 0.02$ m for $d = 0.4$ m and $\pm 0.05$ m for $d = 0.7$ m. Errors in the prescribed ice concentration propagate in the same way as errors in the radiometric accuracy, whereas a 5% error in the concentration would translate to a 7 K error in the brightness temperature. Thus, a 5% ice concentration error would translate into an uncertainty of $\pm 0.1$ m for a thickness of 0.5 m. A 5% error is likely the upper limit of uncertainty for ice concentration retrievals in the central Arctic (Andersen et al., 2007).

## 5.2 Comparison of ice thickness retrievals

The campaign dataset consists of four profiles of nearly coincidental EM and EMIRAD measurements. The analysis of the data is complicated because of the relatively small EM footprint and the spatial displacement between both measurements. In the following, we show the analysis for the flight track with the best spatial overlap of EM and EMIRAD measurements. The vertical channel of the aft looking antenna was heavily degraded for this track. Therefore, we consider the nadir data only.

The sea-ice thickness $d_{\mathrm{TB}}$ was obtained from the brightness temperature by the inversion of the semi-empiric model (Eq. 11) for a prescribed ice concentration $C = 0.98$, salinity $S_{\mathrm{ice}} = 0.65$ and an ice bulk temperature range $T_{\mathrm{ice}} = -2 \pm 1^{\circ}\mathrm{C}$. These assumptions lead to the following three sets of retrieval parameters, $T_0 = 90.8$ K, $T_m = 245.5$ K and $\gamma = 5.9\,\mathrm{m}^{-1}$ for $T_{\mathrm{ice}} = -1^{\circ}\,\mathrm{C}$, $T_0 = 92.4$ K, $T_m = 245.9$ K and $\gamma = 4.0\,\mathrm{m}^{-1}$ for $T_{\mathrm{ice}} = -2^{\circ}\,\mathrm{C}$ and $T_0 = 93.8$ K, $T_m = 245.1$ K and $\gamma = 3.3\,\mathrm{m}^{-1}$ for $T_{\mathrm{ice}} = -3^{\circ}\,\mathrm{C}$.

The resulting thickness is shown in Figs. 5 and 6 together with the smoothed and high frequency EM thickness $d_{\mathrm{EM}}$, an ASAR image and bathymetric data.

Ridged areas and ship tracks that are well visible in the ASAR image are recognized in both thickness retrievals. The darker area in the ASAR image on the right-hand side agrees with retrieved thicknesses between 0.2 and 0.5 m. Gaps in the $d_{\mathrm{TB}}$ curve indicate a failure of the retrieval which could be either explained by ice temperatures higher than $T_{\mathrm{ice}} = -1^{\circ}\mathrm{C}$ or ice thicker than 1.5 m.

The correlation of $d_{\mathrm{EM}}$ and $d_{\mathrm{TB}}$ is 0.5 which indicates a relationship which was very likely (99.7% significance) not caused by chance (Fig. 7). The data points shown in

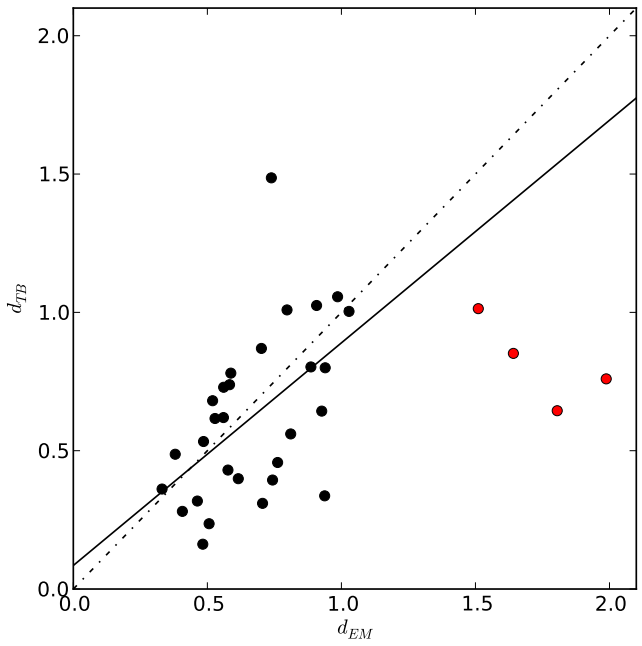


**Fig. 7.** Scatterplot $d_{\mathrm{TB}}$ and $d_{\mathrm{EM}}$ for interpolated averages along the track shown in Fig. 6. Each point represents an average over a section of about 1200 m which is similar to the doubled 3 dB footprint of the EMIRAD instrument. A linear regression yield $d_{\mathrm{TB}} = 0.8 d_{\mathrm{EM}} + 0.08$ m with a standard error of 0.16 and a correlation coefficient of $r = 0.5$ by including only the values with $d_{\mathrm{EM}} < 1.5$ m (black dots). The correlation decreases to $r = 0.1$ by including also the values $d_{\mathrm{EM}} > 1.5$ m (red dots).

Fig. 7 are averages over approximately 1200 m long sections. The overall mean thickness and the standard deviation of the thickness derived from the EM measurement and from the 1.4 GHz radiometry are $d_{\mathrm{EM}} = 0.82 \pm 0.4$ m and $d_{\mathrm{TB}} = 0.65 \pm 0.3$ m, respectively. The EM modal sea-ice thickness amounts to 0.5 m and is significantly smaller than the mean thickness because of the skewness of the thickness distribution. The results agree well with Swedish Meteorological and Hydrological Institute (SMHI) ice maps that indicate level ice thicknesses in the range of 0.15–0.7 m.

## 6 Discussion

### 6.1 Validity of the assumptions

#### 6.1.1 Limitations of the dataset

The results shown in this study represent only a part of the data collected during the SMOS Sea-Ice campaign. We have not presented the remaining data that do not show good correlations. However, these negative results do not have the strength to falsify our conclusions because of the relatively low validity of the measurements. There have been certain limitations with respect to the spatial overlap between the EM and the L-band measurements. The L-band data were seen to be occasionally degraded and the radiometer was not operating at its nominal performance. The EM data was potentially affected by the shallow bathymetry and the sea-ice ridging. Furthermore, no accurate information about the sea-ice temperature was available and the melting conditions were adverse. Thus, our conclusions drawn from the limited dataset are not based on solid ground, or in other words, rest on thin ice. Nevertheless, the relatively good agreement between the model results and the presented data permit to state that the possibility for ice thickness retrieval is given within certain limitations.

#### 6.1.2 Incoherent averaging

In the present study, an incoherent model was tested for retrieval. However, observational UHF (610 MHz) data suggest that coherent effects should possibly be taken into account (Hallikainen, 1983). A major difference between the results of Hallikainen (1983) and the present study is the spatial integration and the used wavelength. The footprint of the UHF measurements was on the order of two magnitudes smaller whereas the wavelength was doubled. Both factors are in favour of interferometric oscillations. When taking a larger integration field into account, the incoherent assumptions are more applicable because of the increased inhomogeneity at the larger scale. We expect that incoherence is a very reasonable assumption for the large scale SMOS FOV. The multi-angle SMOS data should be investigated to study the effect of coherence on the averaging process. This might be possible because different incidence angles translate to different pathlengths through the ice.

#### 6.1.3 Vertical model resolution

The three layer model assumes a homogeneous slab of ice which is a strong simplification. Even if the ice structure, density and salinity would be homogeneous there would still be a vertical temperature gradient resulting from the temperature difference between the atmosphere and the ocean. Multi layer sea-ice models can be employed to investigate these effects. By doing this Tonboe (2009) arrived at a similar conclusion as compared to the present study.

#### 6.1.4 Specular reflection

A specular reflecting surface was assumed for the calculation of the reflectivity and, thus, the emissivity. In general the sea-ice and the ocean do not exhibit a smooth surface. The theory of rough surface or slightly rough surface scattering relies on further assumptions about the stochastic nature of the surface roughness such as the correlation function and the rms height. However, the correlation function is difficult to obtain. If it was available an improved emissivity model could be derived. This would be particularly important for off nadir measurements and to account for the polarization.

### 6.2 Simultaneous ice thickness and concentration retrieval

The question remains open if simultaneous retrievals of ice concentration and thickness will be possible with SMOS data alone. By considering the nadir data only this is definitely not the case. If the multi-angle SMOS data can be used for this purpose this should be further investigated. A more appropriate emission model that accounts for the surface roughness is probably a prerequisite for theoretical studies.

### 6.3 Estimation of retrieval parameters

For the present study the a priori parameters ice concentration, ice salinity and ice temperature were relatively well known. To apply the method for SMOS retrieval the information about ice concentration and temperature could stem from different sensors like AMSR-E. High resolution sea-ice concentration could be aggregated to the SMOS FOV (Spreen et al., 2008). To avoid additional assumptions about ice temperature and, even more difficult, about the ice salinity, the retrieval parameters could be constrained when suitable training data are available. The parameters $T_0$ and $T_1$ could be estimated from minimum and maximum values of the observed brightness temperature if there is a completely ice-free and a thick ice-covered footprint in the swath. The coefficient $\gamma$ could be estimated by the means of co-located brightness temperatures and sea-ice thickness data. The regional and seasonal variability of $\gamma$ should be investigated to assess if the assumption of a constant is applicable.

### 6.4 Complementarity of SMOS and CryoSat ice thickness retrieval

Could there be a benefit of combining SMOS and CryoSat data? We describe in the following the error characteristics for both sensors.

The CryoSat sea-ice thickness retrieval will be based on the measurement of sea-ice freeboard. Using a priori information about the snow thickness and the snow and sea-ice densities, the freeboard can be converted into a thickness. We assume a $\pm 1$ cm uncertainty for the freeboard measurement as the only error source. The SMOS retrieval for Baltic sea-ice of $T_{\mathrm{ice}} = -1\,^{\circ}\mathrm{C}$ shall be influenced by a radiometric uncertainty of $\pm 5$ K as the only error source. The resulting relative errors of the retrieval are shown in Fig. 8. It can be seen that a thickness below about 0.4 m the relative error of the SMOS retrieval is smaller than that of CryoSat. It should be stressed that the results shall be interpreted only qualitatively since the error budget is incomplete and only a very rough estimate. However, the main characteristics will remain similar for a more complete and accurate error budget. The shown complementarity could be exploited in a combined dataset from both sensors. The SMOS data should then be taken into account if the ice is indicated to be thinner than 0.4 m. Assimilation systems like that of Kauker et al. (2009) could take advantage of such complementary input data.

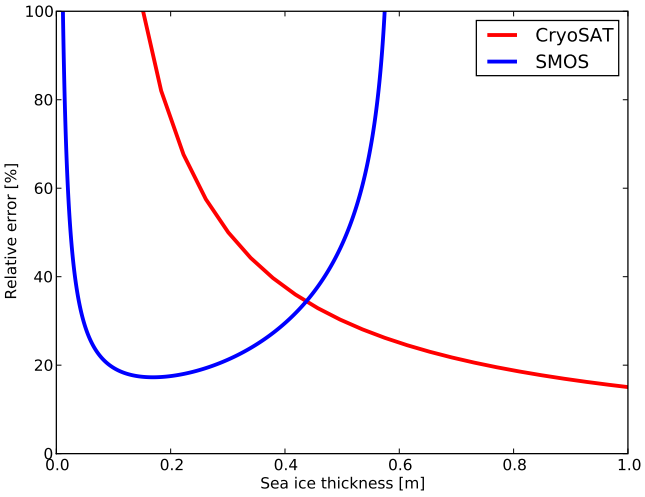


**Fig. 8.** Error characteristic of SMOS and CryoSat ice thickness retrieval for a simplified error budget as explained in the text.

### 6.5 Spatial and temporal resolution

It is instructive to compare the SMOS spatial resolution to those of the Special Sensor Microwave/Imager (SSM/I) because its performance has been widely assessed. The SMOS nadir resolution of 35 km is similar to the SSM/I 37 GHz channel. In a far range the SMOS 80 km footprint is slightly larger than along the track resolution of the SSM/I 19 GHz channel. The SSM/I has been a tremendously important system for sea-ice application despite its relatively coarse resolution. The good temporal sampling and spatial coverage outweigh the drawbacks of the coarse resolution in many cases. A major limitation of the coarse resolution is the restricted application in coastal areas due to the land spillover effect. These influences can possibly be reduced by an unmixing technique (Maaß and Kaleschke, 2010).

### 6.6 Seasonal restriction

With the onset of melt, the ice thickness retrieval will probably be impossible with SMOS due to the strongly reduced penetration depth. Therefore, the SMOS retrieval shall be restricted to the cold seasons. A promising field for the SMOS application would be the observation of young ice growth that is only poorly achievable with existing satellite sensors.

## 7 Conclusions

The new SMOS L-band radiometer was recently launched and NASA's Aquarius mission is awaiting its launch. We described a model for the retrieval of ice thickness from L-band

radiometric data. We tested it against aircraft measurements of 1.4 GHz brightness temperature and coincident ice thickness data derived using electromagnetic induction.

The incoherent model solution (Fig. 1) shows a monotonic increase of brightness temperature for increasing ice thickness. This allows calculating the sea-ice thickness from the measured brightness temperature by a simple inversion of the function for prescribed free parameters. The model degrees of freedom are limited and the needed information can be obtained from other satellites, e.g., the ice concentration and the ice temperature from AMSR-E, or can be parameterized. The most important model parameters besides incidence angle, ice thickness and ice concentration are the ice surface roughness, the ice bulk temperature and the ice bulk salinity. Variations in ocean salinity and temperature can be neglected for this application because of the large radiometric contrast between ice and water. A parameterization of the sea-ice roughness as a percentage of ice thickness seems to be a reasonable approach. New measurements are necessary to validate this parameterization.

The SMOS Sea-Ice campaign was conducted under adverse melting conditions which led to a small thickness sensitivity of the ice emissivity. Towards larger ice thickness the retrieval error becomes infinitely large. We suggest that the retrieval should be interpreted as a lower boundary of the thermodynamic (i.e., modal or level) ice thickness. The retrievable maximum ice thickness is constrained by the ice temperature and salinity.

Overall, this study supports the expectation that the new spaceborne 1.4 GHz radiometers can be used to measure ice thickness. Our model results suggest that the upper limit for the sea-ice thickness retrieval will be roughly half a metre for the Arctic and 1.5 m for the Baltic.

More ice thickness measurements are needed for the validation. The time and position of future validation campaigns is uncritical because of the good spatiotemporal coverage of the SMOS data which is a great advantage as compared to altimeters.

Thin ice plays an important role for heat exchange between the ocean and the atmosphere. Therefore, an ice thickness product based on L-band radiometry will probably be useful for sea-ice applications in climate research and meteorology, as well as possibly for ship navigation in polar waters and would be complementary to the thickness derived from altimetric freeboard measurements.

*Acknowledgements.* We thank J. E. Balling and N. Skou for the provision of the EMIRAD data, J. Karvonen and M. Similä (FIMR) for the provision of ASAR data, meteorological information and photographs. We thank C. Mätzler for the discussion. We thank the editor T. Zhang and two anonymous reviewers for their comments and suggestions. The work was funded by ESA under Contract 21130/08/NL/EL.

Edited by: T. Zhang

## References

Andersen, S., Tonboe, R., Kaleschke, L., Heygster, G., and Pedersen, L. T.:Intercomparison of passive microwave sea-ice concentration retrievals over the high-concentration Arctic sea-ice, J. Geophys. Res, 112, C08004, doi:10.1029/2006JC003543, 2007.

Corbella, I., Duffo, N., Vall-llossera, M., Camps, A., and Torres, F.: The visibility function in interferometric aperture synthesis radiometry, IEEE T. Geosci. Remote, 42(8), 1677–1682, 2004.

Cox, G. and Weeks, W.: Equations for determining the gas and brine volumes in sea-ice samples, J. Glaciol., 29, 306–316, 1983.

Dinnat, E. P. and Boutin, J.: Issues concerning the sea emissvity modeling at L band for retrieving surface salinity, Radio Sci., 38, 8060, doi:10.1029/2002RS002637, 2003.

Feltham, D. L.: Sea Ice Rheology, Annu. Rev. Fluid Mech., 40, 91–112, doi:10.1146/annurev.fluid.40.111406.102151, 2008.

Frankenstein G. and Garner, R.: Equations for determining the brine volume of sea-ice from −0.5C to −22.9C, J. Glaciol., 6(48), 943–944, 1967.

Granskog, M., Leppäranta, M., Kawamura, T., Ehn, J., and Shirasawa, K.: Seasonal development of the properties and composition of landfast sea-ice in the Gulf of Finland, the Baltic Sea, J. Geophys. Res, 109(C2), C02020, doi:10.1029/2003JC001874, 2004.

Hallikainen, M. and Winebrenner, D. P.: The physical basis of sea-ice remote sensing, in: Microwave remote sensing of sea-ice, edited by: Carsey, F. D., AGU Monograph, 68, Am. Geophys. Union, Washington, DC, 29–46, 1992.

Haas, C.: Airborne EM sea-ice thickness profiling over brackish Baltic sea water, Proceedings of the 17th international IAHR symposium on ice, 21–25 June, 2004, vol. 2, All-Russian Research Institute of Hydraulic Engineering (VNIIG), Saint Petersburg, Russia, 12–17, available at: http://epic.awi.de/Publications/Haa2004c.pdf, 2004.

Haas, C., Lobach, J., Hendricks, S., Rabenstein L., and Pfaffling, A.:Helicopter-borne measurements of sea-ice thickness, using a small and lightweight, digital EM bird, J. Appl. Geoph., 67(3), 234–241, 2009.

Hallikainen, M.T.: A new low-salinity sea-ice model for UHF radiometry, Int. J. Remote Sens., 4655–681, 1983.

Heygster, G., Hendricks, S., Kaleschke, L., Maaß, N., Mills, P., Stammer, D., Tonboe, R. T., and Haas, C.: L-Band Radiometry for Sea-Ice Applications, Final Report for ESA ESTEC Contract 21130/08/NL/EL, Institute of Environmental Physics, University of Bremen, available upon request from ESA, 2009.

Hendricks, S. and Haas, C.: WP 2.2: POL-ICE campaign: Ice thickness observations, in: L-Band Radiometry for Sea-Ice Applications, Final Report for ESA ESTEC Contract 21130/08/NL/EL, 2009.

Tonboe, R. T.: WP 2.3a Stokes components Tv, Th from combining thermodynamic and emissvity models, in: L-Band Radiometry for Sea-Ice Applications, Final Report for ESA ESTEC Contract 21130/08/NL/EL, 2009.

Kauker, F., Kaminski, T., Karcher, M., Giering, R., Gerdes, R., and Voßbeck, M.: Adjoint analysis of the 2007 all time Arctic sea-ice minimum, Geophys. Res. Lett., 36, L03707, doi:10.1029/2008GL036323, 2009.

Kerr, Y. H., Waldteufel, P., Wigneron, J. P.,Martinuzzi, J. M., Font, J., and Berger, M.: Soil moisture retrieval from space: The Soil Moisture and Ocean Salinity (SMOS) mission, IEEE T. Geosci.

Remote, 39(8), 1729–1735, 2001.

Klein, L. and Swift, C.: An improved model for the dielectric constant of sea water at microwave frequencies, IEEE J. Ocean Eng., OE-2, 104–111, 1976.

Leppäranta, M. and Manninen, T.: The brine and gas contents of sea-ice with attention to low salinities and high temperatures, Internal Report 2, Finnish Institute of Marine Research, 1988.

Leppäranta, M. and Myrberg, K.: Physical oceanography of the Baltic Sea, Springer Verlag, 2009.

Maaß N. and Kaleschke, L.: Improving passive microwave sea ice concentration algorithms for coastal areas – Applications to the Baltic Sea, Tellus A, 62(4), 393-410, doi:10.1111/j.1600-0870.2010.00452.x, 2010.

Mätzler, C.: Applications of SMOS over terrestrial ice and snow, 3rd SMOS Workshop, DLR, Oberpfaffenhofen, Germany, 10–12 December, 2001.

Maykut, G. A.: Energy exchange over young sea-ice in the central Arctic, J. Geophys. Res., 83, 3646–3658, 1978.

Menashi, J., Germain, K. S., Swift, C., Comiso, J., and Lohanick, A.: Low-frequency passive-microwave observations of sea-ice in the Weddell Sea, J. Geophys. Res, 98, 22569–22577, 1993.

Reul, N., Tenerelli, J., Chapron, B., and Waldteufel, P.: Modeling Sun Glitter at L-Band for Sea Surface Salinity Remote Sensing With SMOS, IEEE T. Geosci. Remote, 45, 2073–2087, 2008.

Rotbøll, J., Søbjærk, S. S., and Skou, N.: A novel L-band polarimetric radiometer featuring sub-harmonic sampling, Radio Sci., 38(3), 8046, doi:10.1029/2002RS002666, 2003.

Spreen, G., Kaleschke, L., and Heygster, G.: Sea-ice remote sensing using AMSR-E 89-GHz channels, J. Geophys. Res., 113, C02S03, doi:10.1029/2005JC003384, 2008.

Swift, C. T.: Passive microwave remote sensing of the ocean – a review, Bound. Lay. Meteorol., 18, 25–40, 1980.

Tenerelli, J., Reul, N., Mouche, A. A., and Chapron, B.: Earth-Viewing L-Band Radiometer Sensing of Sea Surface Scattered Celestial Sky Radiation – Part I: General Characteristics, IEEE T. Geosci. Remote, 46, 659–674, 2008.

Ulaby, F. T., Moore, R. K., and Fung, A. K.: Microwave remote sensing, active and passive. Volume I: Fundamentals and Radiometry, Addison Wesley Pub., London, UK, 1981.

UNESCO: The international system of units (SI) in oceanography, UNESCO Technical Papers No. 45, IAPSO Pub. Sci. No. 32, Paris, France, http://unesdoc.unesco.org/images/0006/000650/065031eb.pdf, 1985.

Vant, M., Ramseier, R., and Makios, V.: The complex-dielectric constant of sea-ice at frequencies in the range 0.1–40 GHz, J. Appl. Phys., 49, 1264–1280, 1978.